2014

Cellular automaton simulation of hot deformation of TRIP steel

Ying Zhi
Northeastern University

Xianghua Liu
Northeastern University, liuxh@uow.edu.au

Hailiang Yu
University of Wollongong, hailiang@uow.edu.au

Cellular automaton simulation of hot deformation of TRIP steel

Abstract

The recrystallization process of hot deformed austenite of TRIP steel was predicted using Cellular Automaton (CA) combined with the principles of physical metallurgy. A model was developed for prediction of the dynamic and static recrystallization microstructure evolution and properties of hot deformed austenite for TRIP steel. The theoretical modeling of recrystallization was based on dislocation density. The microstructure evolution of austenite recrystallization of TRIP steel (such as the grain shape and size, volume fraction, kinetics curve of recrystallization) was predicted both visually and quantitatively. The distribution and variation of the dislocation density and flow stress were also obtained, and the effects of silicon content on recrystallization for TRIP steel were analyzed. The CA calculation results were in good agreement with the measured ones.

Keywords

simulation, automaton, cellular, steel, hot, trip, deformation

Disciplines

Engineering | Science and Technology Studies

Publication Details

Zhi, Y., Liu, X. & Yu, H. (2014). Cellular automaton simulation of hot deformation of TRIP steel. Computational Materials Science, 81 104-112.

Cellular Automaton Simulation of Hot Deformation of TRIP Steel

Ying Zhi [1)], Xianghua Liu [1)], Hailiang Yu [2)]

1) State Key Laboratory of Rolling and Automation, Northeastern University, Shenyang, 110819, China;

2) School of Mechanical, Materials and Mechatronic Engineering, University of Wollongong, Wollongong, NSW 2500, Australia

Abstract: The recrystallization process of hot deformed austenite of TRIP steel was predicted using cellular automaton (CA) combined with the principles of physical metallurgy. A model was developed for prediction of the dynamic and static recrystallization microstructure evolution and properties of hot deformed austenite for TRIP steel. The theoretical modeling of recrystallization was based on dislocation density. The microstructure evolution of austenite recrystallization of TRIP steel (such as the grain shape and size, volume fraction, kinetics curve of recrystallization) was predicted both visually and quantitatively. The distribution and variation of the dislocation density and flow stress were also obtained, and the effects of silicon content on recrystallization for TRIP steel were analyzed. The CA calculation results were in good agreement with the measured ones.

Key words: Cellular Automaton, TRIP steel, recrystallization, flow stress

1. Introduction

Transformation-Induced Plasticity (TRIP) steel is recognized as new generation high-strength steel in the automotive industry [1]. The properties of TRIP steel are largely determined by its microstructure. The microstructure in TRIP steel undergoes complex changes during the hot rolling process. The austenite recrystallization behavior of TRIP steel during hot deformation is an important influencing factor that determines the microstructure and properties [2-3]. Compared with the normal C-Mn steel, TRIP steel has high Si content. This affects the dynamic and static recrystallization behavior during hot deformation, as are the evolution of flow stress and recrystallization fraction. The recrystallization evolution of the C-Mn steel has been the subject of extensive previous research [4], and the mathematical model of prediction of microstructure and properties has been established. However, the quantitative research on the austenite recrystallization behavior of TRIP steel during hot deformation is has received much less attention. In recent years, Cellular Automaton (CA) simulation has been applied to materials research, resulting in the simulation of the metal solidification and recrystallization [5-7] and transformation [8-10]. The prediction of the microstructure evolution of metal using CA has become a hot issue of the international frontier research [11-13]. Therefore, the development of method used to predict the evolution of austenite recrystallization of TRIP steel during hot deformation is greatly significant. In this paper, the combination

methods of the principles of physical metallurgy and CA were adopted, and a programming was carried out on the platform of MATLAB. The dynamic and static recrystallization process of hot deformed austenite of TRIP steel was predicted. The microstructure evolution of austenite recrystallization was simulated quantitatively, such as the grain shape and size, volume fraction and kinetics curve of recrystallization, were visually described. Moreover the distribution and variation of the dislocation density and flow stress were obtained.

2. Prediction of Recrystallization for TRIP Steel

2.1 Mathematical Model of Dynamic Recrystallization

Stuwe et al [14] proposed a theoretical model of dynamic recrystallization based on the dislocation density. Dynamic recrystallization nucleation is associated with the accumulation of dislocation density which increases with increasing strain during the hot deformation process. In the model, it is assumed that recrystallization nucleation occurs at the grain boundary when the dislocation density reaches a critical value, and then the dislocation density begins to decrease. Subsequently, the new grains grow at a certain rate, and their dislocation density increases with increasing the strain. The grains stop growing when the driving force for grain growth is reduced to zero or when the recrystallized grains collide other new grains.

During hot deformation, work-hardening of the metal and dynamic recovery processes occur simultaneously. On the one hand, as the strain increases, work-hardening causes the dislocation density to rise. On the other hand, dynamic recovery causes a reduction in the dislocation density. Burgstrom [15-16] proposed the following relationship between the dislocation density and work hardening and dynamic recovery:

$$\mathrm{d}\rho / \mathrm{d}\varepsilon = U - \Omega \cdot \rho \tag{1}$$

where U and Ω are characteristic parameters of work-hardening and dynamic recovery respectively, ε is the true strain, and ρ the dislocation density.

Dynamic recrystallization occurs during the deformation process when the strain reaches the critical strain value ε_{c} and the dislocation density reaches the critical value ρ_{c}. The critical strain ε_{c} can be expressed as follows [17],

$$\varepsilon_{\mathrm{c}} = 0.83\varepsilon_{\mathrm{p}} \tag{2}$$

where

$$\varepsilon_{\mathrm{p}} = A d_0^q Z^m \tag{3}$$

$$Z = \dot{\varepsilon} \exp[Q_{\mathrm{D}} /(RT)] \tag{4}$$

In Equations (3) and (4), *A*, *q* and *m* are material parameters, ε_{p} is the peak strain, Z the Zener-Hollomen parameter [17], d_0 the austenite grain diameter, R the gas constant, T the absolute temperature, Q_{D} the activation energy for dynamic recrystallization. Q_D can be expressed in terms of the mass percentages of micro-alloy components as [18]:

$$\begin{aligned} Q_{\mathrm{D}} = 267000 - 2535.52[\mathrm{C}\%] + 1010[\mathrm{Mn}\%] + 33620.76[\mathrm{Si}\%] + 35651.28[\mathrm{Mo}\%] \\ + 93680.52[\mathrm{Ti}\%]^{0.5919} + 31673.46[\mathrm{V}\%] + 70729.85[\mathrm{Nb}\%]^{0.5649} \end{aligned} \tag{5}$$

The relationship between the flow stress and the dislocation density can be described as [19]:

$$\sigma = \alpha \mu b \sqrt{\overline{\rho}} \tag{6}$$

where α is the interaction coefficient of dislocation density, usually taken as 0.5, b is the Burgers vector, $\overline{\rho}$ the average dislocation density, and μ the shear modulus.

The nucleation rate $\dot{N}$ is affected by the strain rate and the temperature, and can be expressed as [20, 21]:

$$\dot{N} = C\dot{\varepsilon} /(bl) \exp[-Q_{\mathrm{D}} /(RT)] \tag{7}$$

where C is a constant, $\dot{\varepsilon}$ the strain rate, l the dislocation displacement (also called subgrain size).

The grain growth rate v can be expressed as follows [22]:

$$v = m \cdot P \tag{8}$$

where m is the grain boundary mobility, P is the driving force for grain boundary movement, which in turn can be expressed as [22]:

$$P = 0.5 \rho \mu b^2 \tag{9}$$

2.2 Mathematical Model of Static Recrystallization

The occurrence of static recrystallization requires a certain incubation period, which can be expressed as [23]:

$$\tau = \tau_0 \cdot d_0^{m_\tau} \cdot \dot{\varepsilon}^{n_\tau} \cdot \varepsilon^{l_\tau} \exp[Q_\tau /(\mathrm{R}T)] \tag{10}$$

where τ_0, m_τ, n_τ and l_τ are constants, Q_τ is the surface activation energy.

After hot deformation in the TRIP steel, the static recovery and static recrystallization causes a reduction in the dislocation density. Equation (11) gives the relationship between the dislocation density and static recovery [24],

$$\mathrm{d}\rho/\mathrm{d}t = -k\cdot(\rho-\rho_0)^n \tag{11}$$

where k is the influence coefficient of static recovery. This, in turn, can be expressed as [25],

$$k = k_0\cdot d_0^{m_\mathrm{k}}\cdot\exp(-Q_\mathrm{k}/(RT)) \tag{12}$$

where k_0, m_k, and Q_k are constants. From Equations (11) and (12), the model of the dislocation density is obtained:

$$\rho = (\rho_\mathrm{d}-\rho_0)\cdot\exp(-k\cdot t)+\rho_0 \tag{13}$$

where ρ_d is the dislocation density just in the end of deformation.

The nucleation rate $\dot{N}$ is affected by the strain rate and the temperature, which can be expressed as [26]:

$$\dot{N} = C\dot{\varepsilon}/(bl)\exp[-Q_\mathrm{S}/(RT)] \tag{14}$$

where C is a constant, $\dot{\varepsilon}$ the strain rate, b the Burgers vector, l the dislocation displacement (subgrain size), and Q_S the activation energy for static recrystallization. Q_S can be expressed in terms of the mass percentages of the components as [3],

$$\begin{aligned} Q_\mathrm{S} &= 124714 + 28385.68[\mathrm{Mn}] + 64716.68[\mathrm{Si}] + 72775.4[\mathrm{Mo}] \\ &\quad + 76830.32[\mathrm{Ti}]^{0.123} + 121100.37[\mathrm{Nb}]^{0.10} \end{aligned} \tag{15}$$

where Mn, Si, Mo, Ti and Nb are the mass percentages of Manganese, Silicon, Molybdenum, Titanium and Niobium in the TRIP steel respectively.

During hot deformation, the strain-induced precipitation behavior of low carbon Nb-steel can significantly inhibit static recrystallization. During the isothermal deformation and thermal holding, the softening rate curve reaches a plateau, and the temperature at the beginning of the plateau is defined as the static recrystallization critical temperature (SRCT). The non-recrystallization temperature (T_{nr}) defined by Jonas [27] is roughly the same as the SRCT, which is defined as the start temperature of inhibition recrystallization. Through the analysis of experimental data and regression in reference [28], the relationship between T_{nr} and alloy composition has been obtained,

$$\begin{aligned} T_\mathrm{nr} &= 845 + 54[\mathrm{C}] + 36[\mathrm{Si}] + 43[\mathrm{Al}] + 988[\mathrm{Ti}] \\ &\quad + 4750[\mathrm{Nb}] - 644\sqrt{[\mathrm{Nb}]} + 720[\mathrm{V}] - 240\sqrt{[\mathrm{V}]} \end{aligned} \tag{16}$$

where, as before, C, Si, Al, Ti, Nb and V are respectively the mass percentages of the micro-alloyed components

(Carbon, Silicon, Aluminium, Titanium, Niobium and Vanedium) in the TRIP steel.

2.3 CA Model of Dynamic Recrystallization

A two-dimensional computational domain representing 0.5 mm × 0.5 mm actual sample size was constructed. This is divided into 250 000 (500 × 500) square computational cells, so that each cell side is 1 μm. The isotropic initial grain growth is represented in gray, and newly generated grains are represented in multiple colors. Alternant Moore-type neighbors [29] and periodic boundary conditions are used in the model.

For each cell, four state variables are solved for:

(1) dislocation density (initial value 1.0E12/m^2 [30]): this increases with strain, and decreases upon recovery and recrystallization;

(2) grain orientation: a newly generated recrystallization cell is randomly given a number between 1 and 180 as orientation value. The cell with the same orientation value belongs to the same grain, and different grains are represented by different colors;

(3) recrystallization flag: “0” indicates an un-recrystallized state, and “1” indicates recrystallized state;

(4) grain boundary sign: it is used to indicate the location of grain boundary cell.

The nucleation rule of a certain rate is adopted, and it is assumed that the nucleation occurs only in the cell which has the critical value of dislocation density and is inside the grain boundary. Once nucleation starts in a cell, it will spread to its neighbor at a speed v, changing the neighbor cell from an un-recrystallized state to a recrystallized state.

A deterministic growth rule is adopted, and the grain growth rate can be calculated using Eq. (8). The growth distance l of the nucleated cell to a neighboring un-recrystallized cell can be expressed as:

$$l = \int_0^t v\mathrm{d}t \tag{17}$$

where dt is the time step. If $l \geq a$ (cell dimension), the neighboring un-recrystallized cell will transform into a recrystallized cell.

2.4 Prediction of Recrystallization Parameter

The programming for predicting the recrystallization was carried out on the MATLAB platform, using the principles of physical metallurgy and CA models. The evolution in grain morphology and recrystallization can be traced at different instants of time. The fraction of dynamic recrystallization X_{drx} can be expressed as:

$$X_{drx} = Y_{dr} / Y \tag{18}$$

where Y_{dr} is the number of cells undergoing dynamic recrystallization, and Y is the total number of cells in the adjacent space.

The fraction of static recrystallization X_{srx} can be expressed as follows:

$$X_{srx} = Y_{sr} / Y \tag{19}$$

where Y_{sr} is the number of cells undergoing static recrystallization.

The average grain size of recrystallization in the program was counted and computed based on the assumption that the same grain contains multiple cell area. The dislocation density of every cell at every moment can be predicted, and the changes of the flow stress with the strain also can be obtained according from Eq. (6).

3 Results and Discussion

3.1 Simulation parameters

Using the above method, the austenite recrystallization process of the TRIP steel during the hot deformation was predicted. The chemical composition of the steel is shown in Table 1. Steel A is the TRIP steel with high silicon content, and the steel B is a reference steel with low silicon content. The temperature is assumed to be 1200℃, along with a soaking time of 3 minutes, and the initial grain size of about 82 μm. Table 2 shows the parameters of single-pass compressive deformation for steel A and B in the analysis process.

Table 1 Chemical composition of steel used (mass, %)

Table 2 Parameters of single-pass compressive deformation for steel A and B

Table 3 shows the parameters of double-pass compressive deformation for steel A in the analysis process.

Table 3 Parameters of double-pass compressive deformation for steel A

3.2 Results and discussion

3.2.1 Simulation Results of Dynamic Recrystallization

Based on the parameters of single-pass compressive deformation, the dynamic recrystallization microstructure evolution and property of hot deformed austenite for steels A and B were simulated. The main predicted results are as follows.

1) Microstructure evolution

Fig. 1 shows the predicted results of the microstructure evolution of the dynamic recrystallization of steel A at

the deformation temperature of 1100°C, a strain rate of 0.1 s^{-1}, and different strains. In the figure, it can be seen that dynamic recrystallization nucleation starts at the grain boundary, and then the recrystallized grain continues to grow. The recrystallization fraction increases gradually with increasing strain. The initial austenite grain of austenite is shown in gray, and the newly generated dynamic recrystallized grain is shown in multiple colors.

Fig. 1 Microstructure evolution of dynamic recrystallization for steel A compressed at 1100°C with 0.1s^{-1} rate

Fig. 1 shows only selected pieces of a typical image obtained from the CA simulation of dynamic recrystallization evolution. In fact, the results by CA simulation appear in the form of a dense collection of images at successive time steps, based on the chosen time step Δt. A time series of such images is displayed on the computer screen (or other display device), so that people can visually experience the dynamic, continuous grain nucleation and growth process, until the dynamic recrystallization process is finished. This study provides a whole new way of carrying out a detailed study of the evolution of dynamic recrystallization process

Fig. 2 shows a comparison of the predicted microstructures resulting from the dynamic recrystallization of steel A and steel B at the deformation temperature of 950°C , strain rate 0.1 s^{-1}, and strain 0.69. It is seen that the fraction of dynamic recrystallization for steel A is far less than that for steel B. This is because steel A has high silicon content compared to steel B. The results show that dynamic recrystallization of TRIP steel is inhibited because of high silicon content.

Fig. 2 Microstructure of dynamic recrystallization for steel A and B compressed at 950°C with 0.1s^{-1} rate and 0.69 strain

2) Prediction of the kinetics curve

The predicted S-shaped kinetics curve and the Avrami curve of dynamic recrystallization for steel A with a strain rate of 0.1s^{-1} are shown in Fig. 3 (a) and (b) respectively. In Fig. 3 (b), the 't_r' is the incubation period for the dynamic recrystallization, which indicates that the dynamic recrystallization does not occur at the beginning of the deformation, but over a period of time. As the strain increases, the dislocation density increases to a critical value, and then the nucleation begins. Fig. 3(a) shows that under the same conditions of strain rate, the incubation period of dynamic recrystallization becomes smaller with increasing deformation temperature, and that dynamic recrystallization occurs more easily. From the Avrami curve of dynamic recrystallization in Fig. 3 (b), at different temperature, the Avrami curve shows a linear, and the slope of the line is basically the same which approximately equals to 2 that is consistent with JMAK theory [31] that the two-dimensional growth time index n.

Fig. 3 Kinetics curve of dynamic recrystallization of steel A compressed at strain rate 0.1s^{-1}

3) Prediction of dislocation density

Fig. 4 shows the distribution of dislocation density of steel A at different strains at a deformation temperature 1100℃ and a strain rate of $0.1s^{-1}$. Fig. 1(a) to (d) show that for the grain of beginning nucleation of dynamic recrystallization, the dislocation density obviously decreases, and then the dislocation density of new generated grain increases with increasing strain. As the new grains continue to grow, the dislocation density of cell later undergoing recrystallization in succeeding process is significantly reduced. Inside each dynamic recrystallization grain, the dislocation density shows a decreasing trend from grain interior to grain boundary.

Fig. 4 Distribution of dislocation density (m^{-2}) for steel A compressed at 1100°C with $0.1s^{-1}$ rate

Fig. 5 shows a comparison of predicted results of the distribution of dislocation density of the steel A and steel B at the deformation temperature of 950℃, a strain rate of $0.1s^{-1}$, and strain 0.69. From the figure, it can be seen that the dislocation density of the steel A is far greater than the steel B. It is seen that the dynamic recrystallization of steel A is inhibited due to high silicon content, and the dislocation density is higher.

Fig. 5 Distribution of dislocation density for TRIP steel A (a) and B (b) compressed at 950°C with 0.1 s^{-1} rate and strain 0.69

Fig. 6 shows predictions of the average dislocation density curves of the steel A at different deformation temperatures, and a strain rate of $1s^{-1}$. It can be seen from Fig. 6 that the average dislocation density increases with increasing strain at the beginning of hot deformation. When the dislocation density reaches a critical value, the dynamic recrystallization occurs at the grain boundary and the dislocation density begins to decrease. During hot deformation, work-hardening of the metal and dynamic recovery processes occur simultaneously. As the strain increases, on the one hand, work hardening causes the dislocation density to rise. On the other hand, dynamic recovery causes a reduction in the dislocation density.

Fig. 6 The curve of average dislocation density of steel A during deformation with $1s^{-1}$ strain rate

4) Prediction of flow stress

Fig. 7(a) shows the flow stress curves predictions of the steel A at different deformation temperatures, and a strain rate of $0.1s^{-1}$. The lower the temperature, the greater the flow stress, and plastic deformation is more difficult. Figure 7(b) shows experimental results under the same conditions obtained by Zhu [28]. There is good agreement between the simulation results and experimental results. The predicted flow stress reflects the basic features of the flow stress-strain curves.

Fig.7 Comparison of simulated and measured flow stress curve for steel A compressed with $0.1s^{-1}$ strain rate

Fig. 8 shows the comparison of the flow stress curves predictions of the steel A and B at deformation temperature 950℃ and 1100℃ with a strain rate of $0.1s^{-1}$. At the same deformation temperature, the higher the silicon content, the greater the flow stress.

Fig.8 Comparison of flow stress curves of steels A and B compressed at temperature 950°C and 1100°C with $0.1s^{-1}$ strain rate

5) Prediction of grain size

Fig. 9 shows the average predicted grain size in steel A with different strain rates and deformation temperatures, at a strain of 0.69. At the same strain rate, the average grain size of dynamic recrystallization is larger when the deformation temperature is higher. At the same deformation temperature, the average grain size of dynamic recrystallization is larger when the strain rate is smaller. The reason is that the higher the deformation temperature, and the smaller strain rate, and dynamic recrystallization occurs more easily.

Fig. 9 Mean grain size of dynamic recrystallization for steel A

3.2.2 Simulation Results of Static Recrystallization

Based on the parameters of double-pass compressive deformation, the static recrystallization microstructure evolution and property after hot deformation for steel A were simulated. The main predicted results are as follows:

Fig.10 Microstructure evolution of SRX for steel A after deformation of temperature 1075°C and 5 s^{-1} strain rate

1) Prediction of the microstructure evolution

Fig. 10 shows the predicted results of the microstructure evolution of the static recrystallization of steel A after the first pass deformation temperature of 1075℃ , strain rate 5 s^{-1}, strain 0.3. Figures 10(a) to 10(d) show the simulated results at 0 s, 5 s, 20 s and 50 s respectively. In Fig. 10(a), the initial grain of un-recrystallization is shown in gray, and the multicolor grains represent the newly generated dynamic recrystallization grain during the first pass deformation. The fraction of dynamic recrystallization is 0.2%. In subsequent pass , the nucleation of grains which were deformed continue to grow. Figures 10(b) to 10(d) show the occurrence of the nucleation and growth of static recrystallization grains. The multicolor grains represent the newly formed static recrystallization grains. The corresponding fractions of static recrystallization are 22.8% (5s), 41.7% (20s), and 52.2% (50s).

2) Prediction of kinetics curve

Fig. 11 shows the simulated kinetics curve of the static recrystallization of steel A after deformation. As the

deformation temperature and pass interval time increase, the fraction of static recrystallization also increases. It can be seen that when the deformation temperature increases to1100℃, the fraction of static recrystallization is 58.9%. This indicates that the static recrystallization is incomplete, the main reason is that the static recrystallization of TRIP steel is prevented due to the high silicon content in steel A.

Fig.11 Kinetics curve of static recrystallization of steel A with $5s^{-1}$ strain rate

3) Dislocation density for static crystallization

Fig. 12 shows the predicted results of the average dislocation density during the static recrystallization of the steel A after the first pass deformation different temperature, strain rate $1s^{-1}$, strain 0.3. Due to the static recrystallization and static recovery, the average dislocation density decreases. In the same pass interval, the higher the deformation temperature, the average dislocation density is smaller.

Fig. 12 The curve of average dislocation density of static recrystallization of steel A with $1s^{-1}$ strain rate

Fig. 13 shows the distribution of dislocation density of steel A at different pass interval times after the deformation temperature 900℃ and strain rate 1 s^{-1}. It can be seen from Fig. 13 that for the grain of beginning nucleation of static recrystallization, the dislocation density obviously decreases, and then the dislocation density of new generated grain will decrease with the static recovery. As the new grains continue to grow, the dislocation density of cell growing up into a recrystallization in succeeding growth process is significantly reduced. On the whole, in the region of recrystallization occurrence, the dislocation density is significantly reduced.

Fig.13 Distribution of dislocation density (m^{-2}) for steel A during interpass at temperature 900°C and strain rate $1s^{-1}$

4. Conclusions

(1) A model for predicting the dynamic and static recrystallization of hot deformed austenite for TRIP steel was developed using Cellular Automaton (CA). The code was programmed on the MATLAB platform, and was used to quantitatively predict the microstructure evolution of austenite recrystallization, in terms of parameters such as grain shape and size and volume fraction.

(2) The effects of deformation temperature, strain rate, silicon content and other parameters on dynamic and static recrystallization microstructure in the austenite were analyzed.

(3) The distribution and variation of the dislocation density and flow tress were obtained by CA simulation. The

flow stress in dynamic recrystallization of TRIP steel during hot deformation was consistent with the true deformation process. The predicted results were in good agreement with the measured ones.

(4) The simulation results could provide a theoretical reference for the control of the microstructure and properties of TRIP steel.

Acknowledgements

The authors gratefully acknowledge support from the National Natural Science Foundation of China (Grants 51174249, 50974039, 51034009, and the Fundamental Research Funds for the Central Universities (N110407004).

References

[1] X.D.Wang, B.X. Huang, L.Wang, Y.H. Rong, Microstructure and mechanical properties of microalloyed high-strength transformation-induced plasticity steels, Metall. Mater. Trans. A, 39 (2008) 1-7.

[2] Y. M. Wang, M. Y. Li, G. Wei, Control Rolling and Control Cooling of Steel Plates. Beijing: Metallurgical Industry Press, 2007.

[3] L. J. Zhu, D. Wu, X. M. Zhao, Influence of alloying content on microstructure evolution of hot deformed austenite, J Northeastern Univ, 27 (2006) 987-990.

[4] L. J. Zhu, D. Wu X., M. Zhao, P. J. Wang, Prediction of microstructure evolution of Si-Mn TRIP steel during hot rolling, J. Iron Steel Res., 19 (2008) 36-40.

[5] H. W. Hesselbarth, I. R. Gobel, Simulation of recrystallization by cellular automata, Acta Metal., 39 (1991) 2135-2143.

[6] C. H. J. Davies, The effect of neighbourhood on the kinetics of a cellular automaton recrystallisation model, Scripta Metal., 33 (1995)1139-1143.

[7] C. W. Zheng, Y. J. Lan, N. M. Xiao, D. Z. LI , Y. Y. Li, Mesoscale simulation of static recrystallization of hot deformed austenite in a low carbon steel, Acta Metall. Sin., 42 (2006) 474-480.

[8] X. H. Zhan, Y. H. Wei, Z. B. Dong, Cellular automaton simulation of grain growth with different orientation angles during solidification process, J. Mater. Process. Technol., 208 (2008) 1-8.

[9] N. Yazdipour, C. H. J. Davies, P. D. Hodgson. Comp. Mater. Sci. (2008), Vol. 44, pp. 566

[10] D. Z. Li, N. M. Xiao, Y. J. Lan, C. W. Zheng, Y. Y. Li, Growth modes of individual ferrite grains in the austenite to ferrite transformation of low carbon steels, Acta Mater., 55 (2007) 6234-6249.

[11] X. H. Liu, Progress and application of plastic finite element method in metals rolling process, Acta. Metall. Sin., 46(2010) 1025-1033.

[12] F. Chen, Z. S. Cui, J. Liu, W. Chen and S. J. Chen, Mesoscale simulation of the high-temperature austenitizing and dynamic recrystallization by coupling a cellular automaton with a topology deformation technique, Mater. Sci. Eng. A, 527 (2010) 5539-5549.

[13] C. Bos, M. G. Mecozzi, J. Sietsma, A microstructure model for recrystallisation and phase transformation during the dual-phase steel annealing cycle, Comp. Mater. Sci., 48(2010) 692-699.

[14] W. M. Mao, X. B. Zhao. Recrystallization and Grain Growth of Metal. Beijing: Metallurgical Industry Press, 1994.

[15] S. Serajzadeh, A. K. Taheri, An investigation on the effect of carbon and silicon on flow behavior of steel, Mater. Des., 23 (2002) 271-276.

[16] J. M. Cabrera, A. A. Omar, J. J. Jonas, J. M. Prado, Modeling the flow behavior of a medium carbon microalloyed steel under hot working conditions, Metall. Mater. Trans. A, 28(1997) 2233-2243.

[17] S. Serajzadeh, A. K. Taheri, Prediction of flow stress at hot working condition, Mech. Res. Com., 30(2003) 87-93.

[18] L. J. Zhu, D. Wu, X. M. Zhao. Recrystallization modelling of hot deformed Si-Mn TRIP steel, J. Iron Steel Res. Int. 14 (2007) 61-65.

[19] C. W. Zheng, N. M. Xiao, D. Z. Li, Y. Y. Li, Microstructure prediction of the austenite recrystallization during multi-pass steel strip hot rolling: A cellular automaton modeling, Comp. Mater. Sci., 44(2008) 507-514.

[20] S. Mandal, P. V. Sivaprasad, S. Venugopal, K. P. N. Murthy, Constitutive flow behaviour of austenitic stainless steels under hot deformation: Artificial neural network modelling to understand, evaluate and predict, Modell. Simul. Mater. Sci. Eng., 14(2006) 1053-1070.

[21] Y. Lu, L. W. Zhang, X. H. Deng, J. B. Pei, S. Wang, G. L. Zhang, Modeling dynamic recrystallization of pure copper using cellular automaton method, Acta Metall. Sin., 44(2008) 292-296.

[22] H. Hallberg, M. Wallin, M. Ristinmaa, Simulation of discontinuous dynamic recrystallization in pure Cu using a probabilistic cellular automaton , Comp. Mater. Sci., 49(2010) 25-34.

[23] A. Yoshie, H. Morikawa, Y. Onoe, K. Itoh, Formulation of static recrystallization of austenite in hot rolling process of steel plate, Trans. ISIJ. 27(6) (1987)425-431.

[24] R. L. Goetz, V. Seetharaman, Modeling dynamic recrystallization using cellular automata, Scripta Mater, 38(1998) 405-413.

[25] A. Yoshie, T. Fujita, M. Fujioka, Formulation of the decrease in dislocation density of deformed austenite due to static recovery and recrystallization, ISIJ Int, 36 (1996) 474-480.

[26] M. Qian, Z. X. Guo, Cellular automata simulation of microstructural evolution during dynamic recrystallization of an HY-100 steel, Mater. Sci. Eng. A, 365(2004) 180-185.

[27] L. N. Pussegoda, J. J. Jonas, Comparison of dynamic recrystallization and conventional controlled rolling schedules by laboratory simulation, ISIJ Int., 31(1991) 278-288.

[28] L. J. Zhu. Predicting Microstructure and Property of Hot Rolled Low Carbon Si-Mn TRIP Steel Plate. Shenyang: Northeastern University, 2007.

[29] S.G. R Brown, Simulation of diffusional composite growth using the cellular automaton finite difference (CAFD) method, J. Mater. Sci., 33(1998) 4769-4773.

[30] Z. H. Li, Master Dissertation. Northeastern University, Shenyang, 2004.

[31] W. Z. Jin, L. Wang, X. H. Liu, Z. F. Wang, Modeling of cellular automaton method in the simulation of recrystallization, Mater. Mech. Eng., 29 (2005) 10-13.

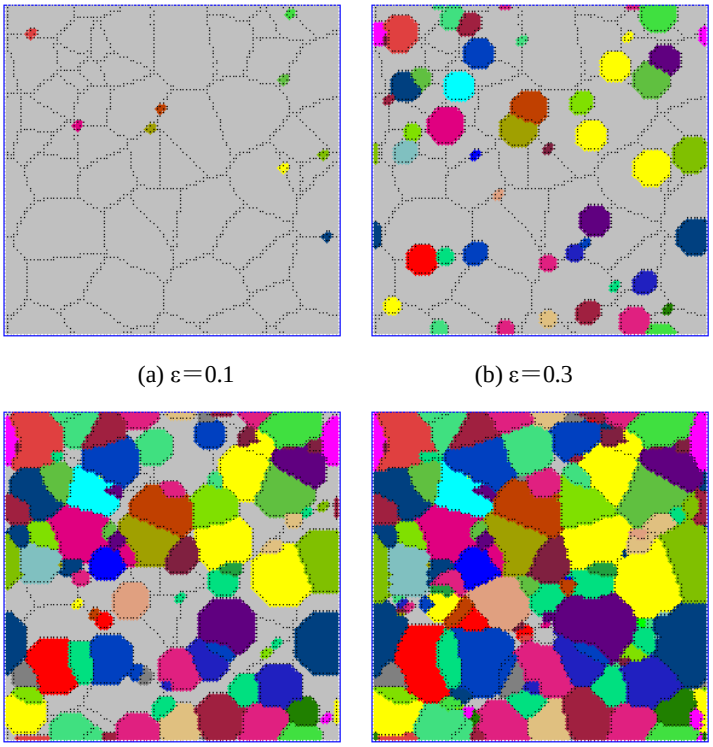

(a) ε＝0.1　　(b) ε＝0.3

(c) ε＝0.5　　(d) ε＝0.69

Fig. 1 Microstructure evolution of dynamic recrystallization for steel A compressed at 1100℃ with $0.1s^{-1}$ rate

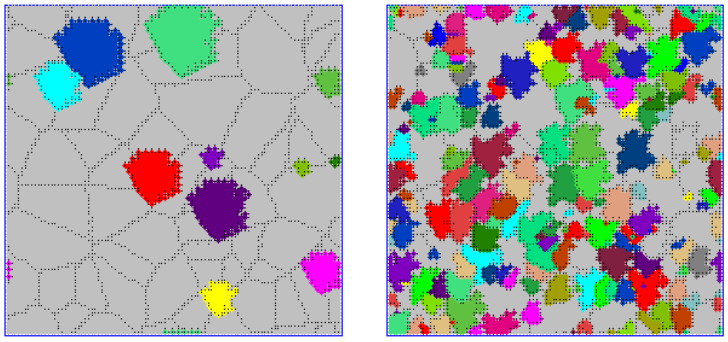

(a) steel A (b) steel B

Fig. 2 Microstructure of dynamic recrystallization for steel A and B compressed at 950°C with $0.1s^{-1}$ rate and 0.69 strain

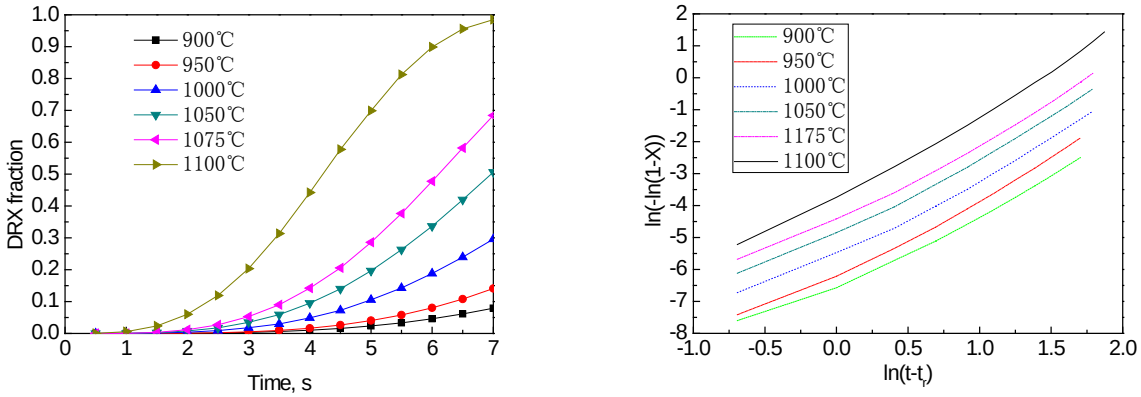

(a) S curve (b) Avrami curve

Fig. 3 Kinetics curve of dynamic recrystallization of steel A compressed at strain rate $0.1s^{-1}$

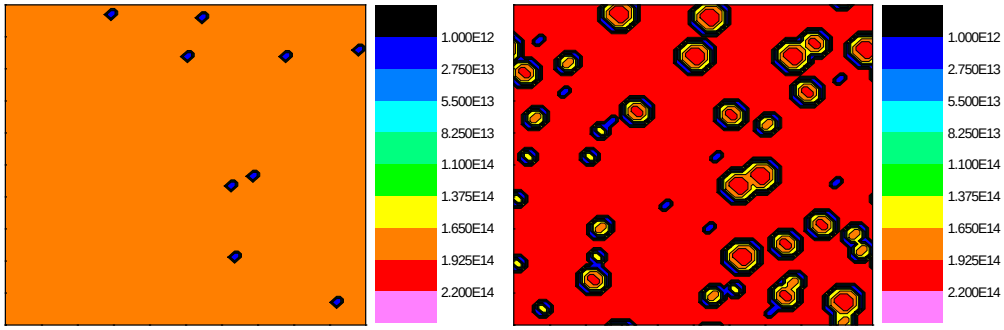

(a) ε＝0.1 (b) ε＝0.3

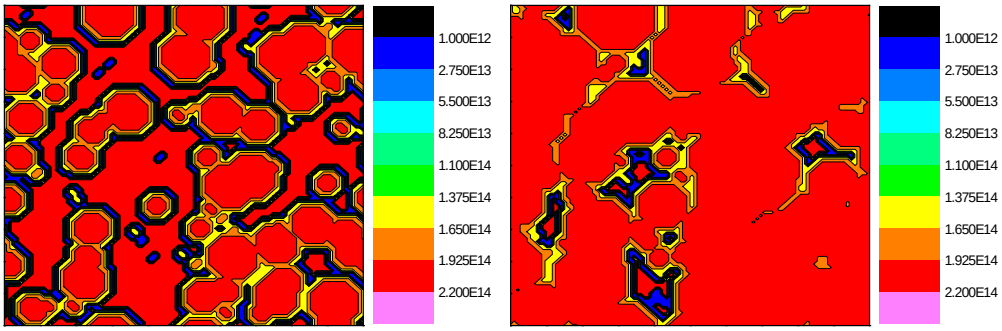

(c) ε＝0.5 (d) ε＝0.69

Fig. 4 Distribution of dislocation density (m^{-2}) for steel A compressed at 1100°C with $0.1s^{-1}$ rate

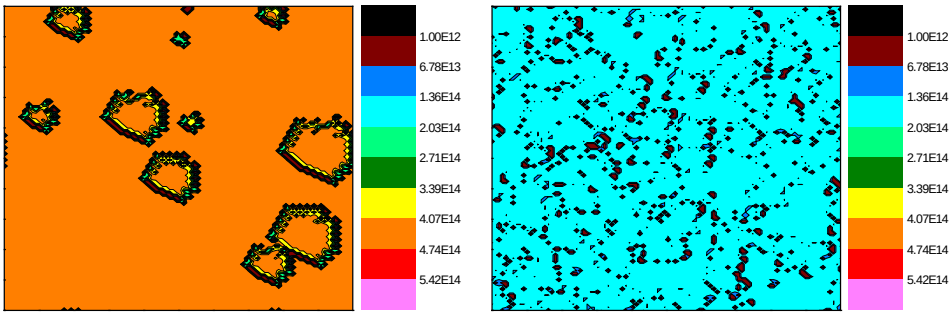

(a) steel A (b) steel B

Fig. 5 Distribution of dislocation density for TRIP steel A (a) and B (b) compressed at 950°C with 0.1 s^{-1} rate and strain 0.69

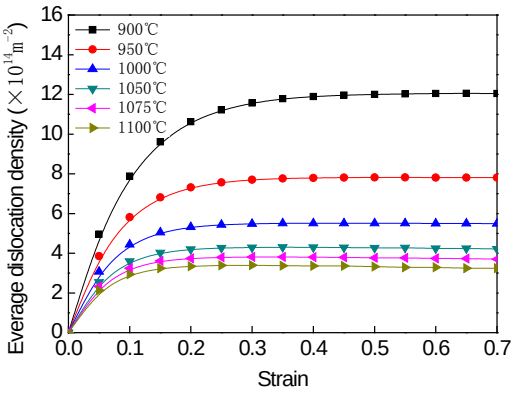

Fig. 6 The curve of average dislocation density of steel A during deformation with $1s^{-1}$ strain rate

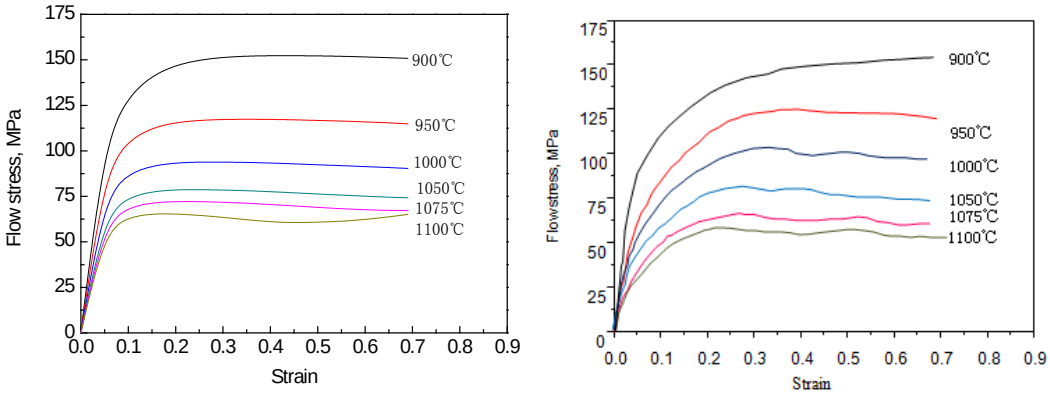

(a) simulated (b) measured[29]

Fig.7 Comparison of simulated and measured flow stress curve for steel A compressed with $0.1s^{-1}$ strain rate

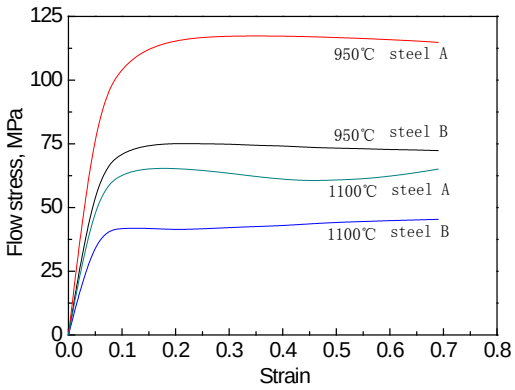

Fig.8 Comparison of flow stress curves of steels A and B compressed at temperature 950°C and 1100°C with $0.1s^{-1}$ strain rate

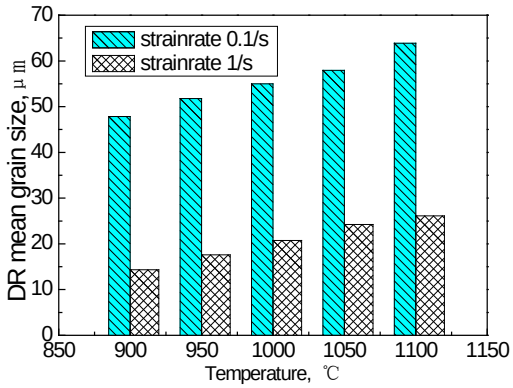

Fig. 9 Mean grain size of dynamic recrystallization for steel A

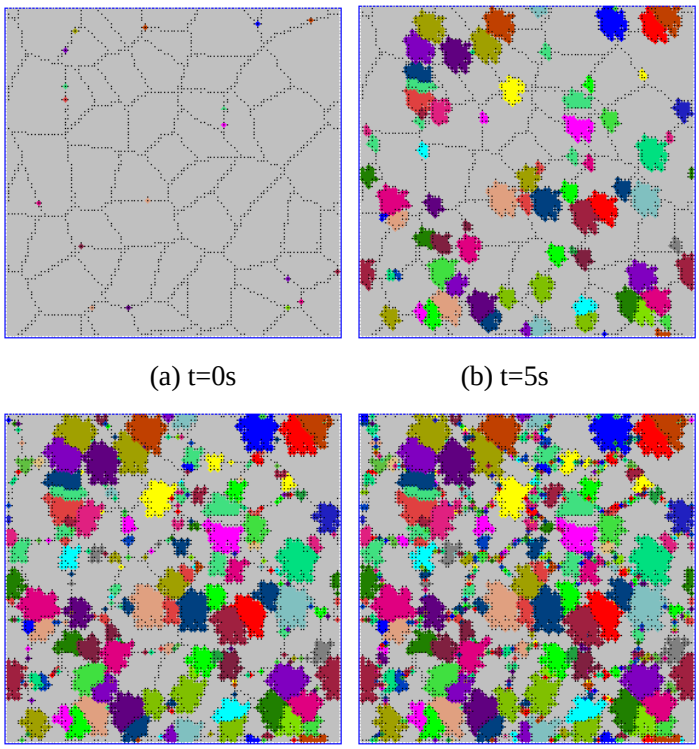

(a) t=0s (b) t=5s

(c) t=20s (d) t=50s

Fig.10 Microstructure evolution of SRX for steel A after deformation of temperature 1075℃ and 5 s^{-1} strain rate

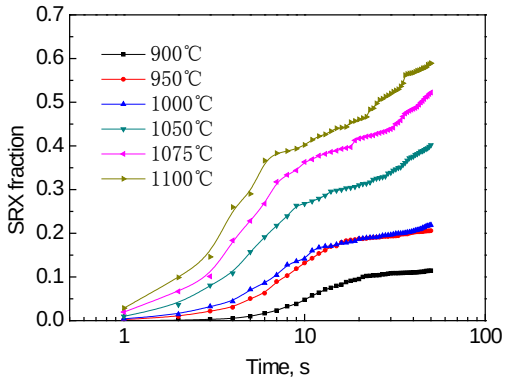

Fig.11 Kinetics curve of static recrystallization of steel A with $5s^{-1}$ strain rate

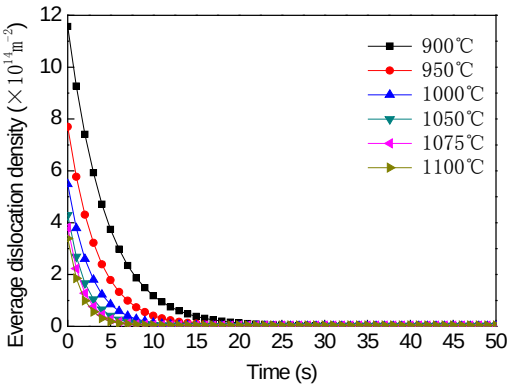

Fig. 12 The curve of average dislocation density of static recrystallization of steel A with $1s^{-1}$ strain rate

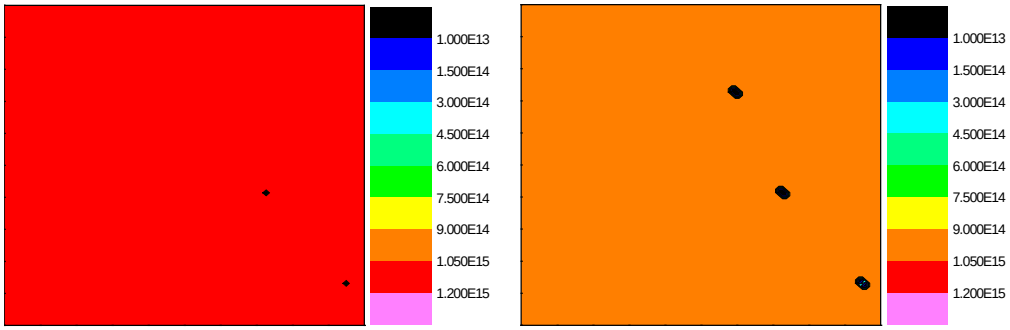

(a) t=0s (b) t=1s

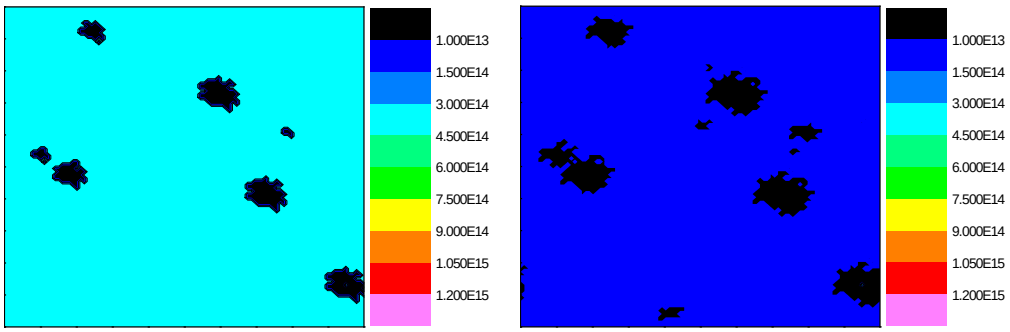

(c) t=5s (d) t=10s

Fig.13 Distribution of dislocation density (m^{-2}) for steel A during interpass at temperature 900°C and strain rate $1s^{-1}$

Table 1 Chemical composition of steel used (mass，%)

Steel	Chemical composition	C	Si	Mn	S	P	Al
A	Mass, %	0.233	1.365	1.54	0.004	0.0074	0.08
B		0.233	0.17	1.54	0.004	0.0074	0.08

Table 2 Parameters of single-pass compressive deformation for steel A and B

Strain rate, s-1	True strain	Deformation temperature, °C
0.1	0.69	900, 950, 1000, 1050, 1075, 1100
1		900, 950, 1000, 1050, 1075, 1100

Table 3 Parameters of double-pass compressive deformation for steel A

Strain rate, s^{-1}	True strain $\varepsilon_1 + \varepsilon_2$	Deformation temperature, °C	Interpass time, s
1 5	0.3+0.3	900~1100	1, 5, 10, 15, 20, 30, 50